Control Strategies of a Single Phase Switched Capacitor Nine-Level Inverter for PV System Applications

Ayoub Nouaiti*‡, Abdallah Saad*, Abdelouahed Mesbahi*, Mohamed Khafallah*

* Laboratory of Energy and Electrical Systems (LESE), Superior National School of Electricity and Mechanical (ENSEM), University of Hassan II Casablanca, Morocco

(nouayoub@gmail.com, saad.abdal@gmail.com, abdelouahed.mesbahi@gmail.com, mohamed.khafallah@uh2c.ma)

‡ Corresponding Author; First Author, Route d'El Jadida, km 7, Oasis – Casablanca 8118, Maroc, Tel: +212522230789, Fax: +212522231299, nouayoub@gmail.com

Received: 23.04.2017 Accepted: 29.05.2017

Abstract- This paper presents the design and simulation of a single phase nine level inverter with two different control strategies for two important PV system applications. The first method combines the maximum power point tracking (MPPT) method with the voltage regulation method, and its concerns the autonomous PV system applications without using batteries. The second method combines the MPPT with the power factor correction, and it's used to tie the studied multilevel inverter with the power grid. This multilevel inverter consists of a DC-DC switched capacitor converter and a simple DC-AC full bridge converter. It generates an AC voltage with nine levels similar to a sinusoidal in shape.

The studied PV system is tested with modelled solar panels in MATLAB/SIMULINK. The obtained simulation results prove that the studied system with the associated control strategies is a good solution for PV pumping system and also for injecting power energy into electrical power grid from PV source. Also, experimental results of a laboratory prototype tested with 130W single phase induction motor driving a water pump are presented for validation of the topology of the studied inverter.

Keywords Multilevel inverter; Switched capacitor converter; Grid tie inverter; Single phase induction motor; Pumping system.

1. Introduction

The renewable energy sources provide many important advantages such as good environmental quality, low maintenance costs, low operating costs, and inexhaustible energy. For the PV systems, the power electronics techniques, and converters play a crucial role, particularly in the conversion of energy from direct current (DC) to alternating current (AC) [1] [2] [3].

The classification of the classical inverters based on the type of the output voltage is square wave inverters, quasi-square wave inverters and two-level PWM inverters. These DC-AC inverters operate at a high switching frequency, with high switching losses. In PV systems the power components of these inverters should block the maximum DC voltages imposed by the photovoltaic chain. Also, in industrial applications, these inverters have the quandary of introducing harmonics in the AC voltages. For that, the machines losses will be high, also their temperature will increase, and this will reduce their efficiency. All these constraints can reduce the robustness and lifetime of these inverters [4]. Multilevel inverters introduce a good solution to surmount the cited problems. Their structure has begun in early 1975 with three-level converters. They are becoming popular due to the reduced voltage across the power switches, less electromagnetic interference, small output filters size, low harmonic distortion. Also, they develop a nearly sinusoidal voltage at their AC output terminal [4] [5] [6]. Classical multilevel inverter topologies can be classified into three categories: Diode Clamped; Neutral Point Clamped multilevel Inverter, Flying Capacitor; Capacitor Clamped multilevel Inverter, Cascaded H-Bridge multilevel Inverter [4] [6] [7] [8]. The problem of unbalanced voltage is present in neutral point clamped, flying capacitor, and capacitor clamped multilevel inverter. For the cascaded H-bridge

inverter structures, no voltage balancing problems, but they require many voltage sources in order to develop the number of the output voltage levels. From these classical structures, different topologies of multilevel inverters are derived by using symmetric, asymmetric and hybrid arrangement [9]. Switched capacitors multilevel inverters are efficient topologies derived with the hybrid arrangement. They offer the possibility to step-up the input voltages just using capacitors without using inductors, and also they deliver optimal AC voltages and currents [10].

This paper presents a single-phase nine level inverter with a switched capacitor converter for PV system applications, with only single DC voltage source from solar panels. This inverter delivers fewer harmonics, has a good output waveform spectrum and overcomes the unbalanced voltage problem across capacitors. The main elements used in the studied multilevel inverter are, a high step-up DC–DC switched capacitor converter derived from a new generalized structure that has been appeared recently in the literature [14], and a classical DC–AC (full bridge) converter. Two control methods for two different PV system applications are presented; the first method is Maximum Power Point Tacking (MPPT) with voltage regulation applied on the studied multilevel inverter delivering power energy from solar panels to autonomous loads and especially for PV pumping system. The second method is MPPT with unity power factor correction applied on the studied multilevel inverter delivering power energy from solar panels into the electrical power grid. Experimental results of a hardware setup of the studied inverter tested on a water pump are presented just for the validity of the topology and its advantages.

The structure of this paper is presented as follows: Section 2 presents the proposed PV system. Section 3 presents the control method of the studied PV system for stand-alone applications with MPPT and voltage regulation. Section 4 presents the control method of the studied PV system tied to the grid with MPPT and unity power factor correction. Section 5 presents simulation results. Sections 6 and 7 present respectively the experimental results and the conclusion.

2. The Proposed PV System

The structure of the studied PV system is shown in "Fig.1". It's based on single DC voltage source from solar panels (Vpv), a DC–DC switched capacitor converter, and a DC–AC (full bridge) converter.

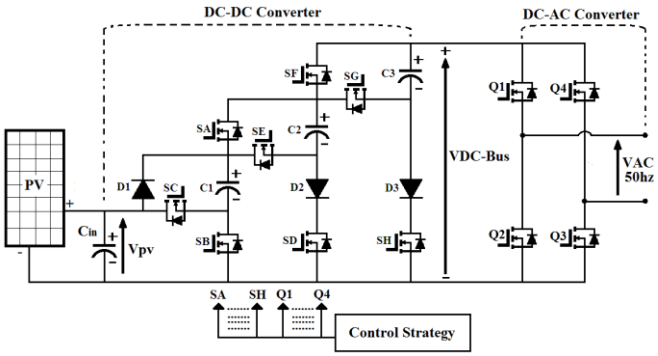

Fig.1. The structure of the proposed PV system

2.1. Solar panels

Solar panels are an assembly of solar cells in series and parallel, which absorb photons from the sun's rays in order to generate electricity through the photovoltaic effect.

The electrical model of a solar cell is presented in "Fig.2". It consists of a current source, single diode, series resistance and a parallel resistance [11] [12] [13].

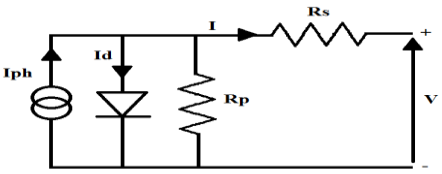

Fig.2. Electrical model of a solar cell

"Eq. (1)" shows the expression of the generated current from the model of a solar cell [11] [12] [13]:

$$I = Iph - Is\left(\exp\frac{q(V+RsI)}{NKT} - 1\right) - \frac{(V+RsI)}{Rp} \qquad (1)$$

Where I is the output current, Iph is the photocurrent, Is is the reverse saturation current of the diode, V is the output voltage, N is the ideality factor of the diode, q is the electron charge (1.60217662×10-19coulombs), T is the junction temperature , and K is the Boltzmann constant (1.38064852 × 10-23 m2 kg s-2 K-1).

The used solar panels in this paper are Solarex-MSX60. The electrical parameters of only one solar panel are shown in "Table 1."

Table 1. Electrical parameters of the used solar panels

Maximum power (Pmax)	60W
Voltage at Pmax (Vmp)	17.1V
Current at Pmax (Imp)	3.5A
Short-circuit current (Isc)	3.8A
Open-circuit voltage (Voc)	21.1V
Number of solar cells	36

The proposed solar panels are modelled in MATLAB/SIMULINK with the help of the "Eq. (1)". "Figure 3" and "Figure 4" show respectively P-V

characteristics, and I-V characteristics for only one solar panel for different irradiation levels and temperatures levels (1000w/m2 with 25°c, 800w/m2 with 20°c, 600W/m2 with 18°c).

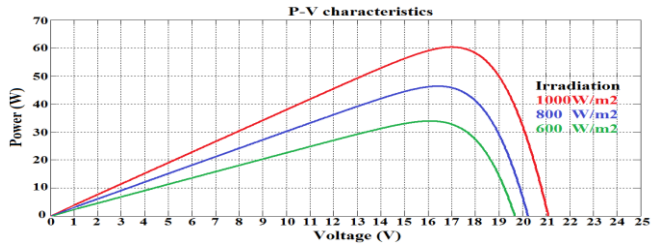

Fig.3. P-V characteristics of one solar panel

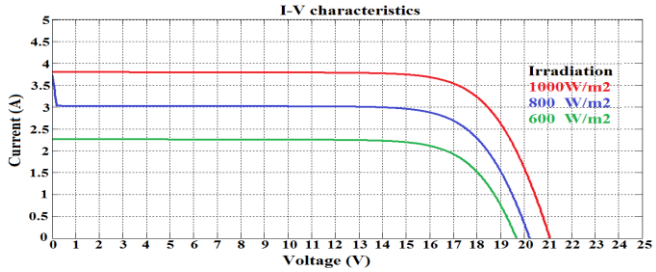

Fig.4. I-V characteristics of one solar panel

2.2. DC-DC switched capacitor converter

The proposed switched capacitor converter is shown in "Fig.5". It is based on the generalized structure proposed in [14] [15]. This converter consists of a single DC power source (Vpv), 8 switches, 3 diodes, and 3 capacitors. It is a DC-DC converter. It provides a DC bus with a high output voltage four times higher than the input voltage (Vpv) with a special shape without using inductors or high-frequency transformer.

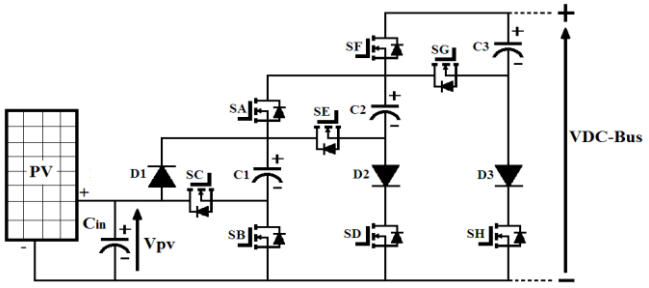

Fig.5. The structure of the DC-DC converter

"Figure 6" shows the different operation modes of the studied DC-DC converter.

In mode I, when the power switches SA, SB and SF are ON (SC, SD, SE, SG and SH are OFF), and the diode D1 is forward biased (D2 and D3 are reversely biased), the capacitor C1 is charged by the input voltage Vpv. In this case, the value of the output DC Bus voltage is:

VDC Bus= VC1= Vpv (2)

In mode II, when the power switches SA, SC, SD and SF are ON (SB, SE, SG and SH are OFF), and the diode D2 is forward biased (D1 and D3 are reversely biased), the capacitor C2 is charged by the input voltage Vpv and also by the voltage VC1 from the capacitor C1 (equation 2). In this case the value of the output DC Bus voltage is:

VDC Bus= VC1+Vpv = 2Vpv (3).

In mode III, when the power switches SE, SF and SH are ON (SA, SB, SC, SD and SG are OFF) and the diodes D1 and D3 are forward biased (D2 is reversely biased), the capacitor C3 is charged by the input voltage Vpv and also by the voltage VC2 from the capacitor C2 (equation 3). In this case the value of the output DC Bus voltage is:

VDC Bus= VC2+Vpv = 3Vpv (4).

In mode IV, when the power switches SA and SG are ON (SB, SC, SD, SE, SF and SH are OFF), and the diode D1 is forward biased (D2 and D3 are reversely biased), the output DC Bus voltage is generated by the input voltage Vpv and also by the voltage VC3 from the capacitor C3 (equation 4). In this case the value of the output DC Bus voltage is:

VDC Bus= VC3+Vpv = 4Vpv (5)

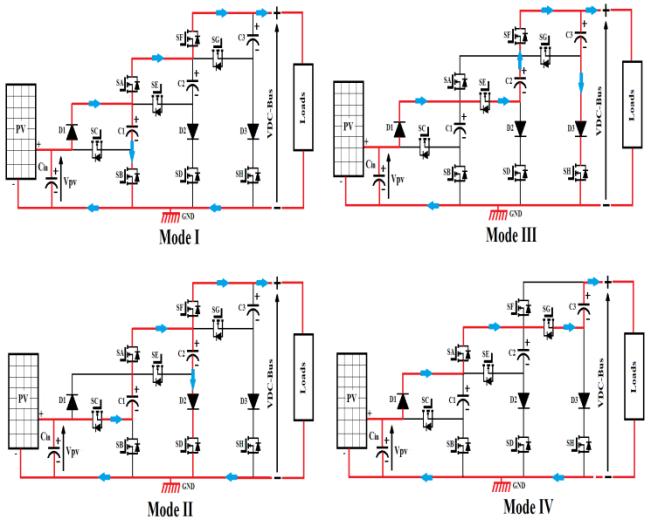

Fig.6. The four operating modes of the proposed DC-DC converter

"Table 2." summarizes the states of the switches and capacitors of the DC-DC converter for a half period. Symbol C means to charge and D means discharge.

The proposed DC-DC converter generates a positive staircase waveform that begins from Vpv and ends at 4Vpv, repeated at each period (T), as shown in "Fig.7".

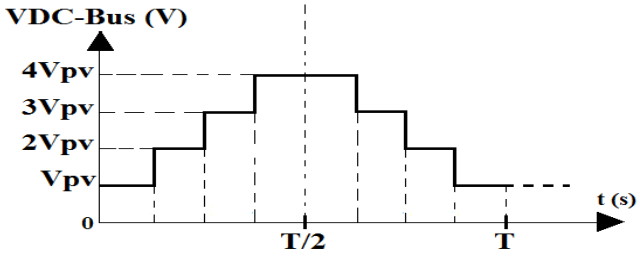

Fig.7. Waveform of the generated DC Bus voltage from the DC-DC converter

2.3. DC-AC (Full Bridge) converter

The used DC-AC converter is shown in "Fig.8". It consists of a single phase H-bridge converter, composed by four switches. Its main function is to convert the DC Bus voltage from the switched capacitor converter to an AC voltage with a chosen frequency (50Hz in this study).

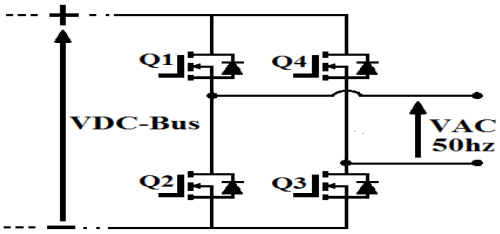

Fig.8. The structure of the DC-AC converter

Table 2. States of the switches and the capacitors of the DC-DC converter

Switches states								Capacitors states			
SA	**SB**	**SC**	**SD**	**SE**	**SF**	**SG**	**SH**	**C1**	**C2**	**C3**	**VDC-Bus**
ON	ON	OFF	OFF	OFF	ON	OFF	OFF	C	-	-	Vpv
ON	OFF	ON	ON	OFF	ON	OFF	OFF	D	C	-	2Vpv
OFF	OFF	OFF	OFF	ON	ON	OFF	ON	-	D	C	3Vpv
ON	OFF	OFF	OFF	OFF	OFF	ON	OFF	-	-	D	4Vpv

Table 3. Switching states of the used power switches

The states of the used switches													
State	**Q1**	**Q3**	**Q4**	**Q2**	**SA**	**SB**	**SC**	**SD**	**SE**	**SF**	**SG**	**SH**	**VAC**
ST5	ON	ON	OFF	OFF	ON	OFF	OFF	OFF	OFF	OFF	ON	OFF	+4Vpv
ST4	ON	ON	OFF	OFF	OFF	OFF	OFF	OFF	ON	ON	OFF	ON	+3Vpv
ST3	ON	ON	OFF	OFF	ON	OFF	ON	ON	OFF	ON	OFF	OFF	+2Vpv
ST2	ON	ON	OFF	OFF	ON	ON	OFF	OFF	OFF	ON	OFF	OFF	+Vpv
ST1	ON	OFF	ON	OFF	ON	ON	OFF	OFF	OFF	ON	OFF	OFF	0
ST6	OFF	ON	OFF	ON	ON	ON	OFF	OFF	OFF	ON	OFF	OFF	0
ST7	OFF	OFF	ON	ON	ON	ON	OFF	OFF	OFF	ON	OFF	OFF	-Vpv
ST8	OFF	OFF	ON	ON	ON	OFF	ON	ON	OFF	ON	OFF	OFF	-2Vpv
ST9	OFF	OFF	ON	ON	OFF	OFF	OFF	OFF	ON	ON	OFF	ON	-3Vpv
ST10	OFF	OFF	ON	ON	ON	OFF	OFF	OFF	OFF	OFF	ON	OFF	-4Vpv

2.4. *Modulation algorithm of the studied PV system*

"Table 3." shows the different switching states (ST) of power switches of the DC-DC converter and the DC-AC converter, with the corresponding voltage levels.

By using the different suggested states described in "Table 3." the proposed PV system will deliver an output voltage (VAC) waveform similar to a sinusoidal in shape with nine levels, as shown in "Fig.9".

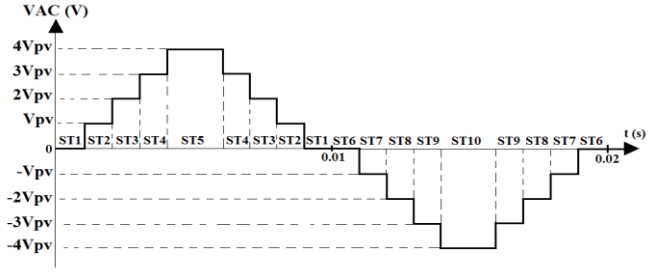

Fig.9. Waveform of the multilevel inverter output voltage

For controlling multilevel inverter structures, two general modulation techniques can be used. The first is based on the high switching frequency, such as space vector modulation (SVM), and pulse width modulation (PWM) which is based on the comparison between high-frequency

carrier signals and sinusoidal signals. The second technique is based on low switching frequency, such as fundamental switching frequency method, and selective harmonic elimination method (SHE) [16] [17] [18].

In order to get the switching pulses for the studied multilevel inverter by considering the switching states, as described in "Table 3." above, a simple pulse width modulation (PWM) control algorithm is applied. This algorithm consists in comparing four identical triangular carrier signals (Carr1… Carr4) (same frequency, same amplitude) in phase and having an offset equal to their amplitude with a reference signal (Ref) which is a rectified sinusoidal (with a frequency of 50Hz), as shown in "Fig.10" [19].

The modulation index (MI) of this method is [19]:

$$MI = \frac{AM}{4AC} \quad (6)$$

AM and AC are respectively the amplitudes of the reference sinusoidal signal and the triangular carrier signal.

"Table 4." resumes the used conditions with the help of logic gates to make the comparisons between the carriers signals and the rectified sinusoidal signal in order to get the output AC voltage shown in "Fig.10" with PWM method, and also for respecting the conditions of the charge and the discharge of the used capacitors in the DC-DC converter as indicated in table 2. Q1 and Q2 are two complementary square wave pulses with a frequency of 50Hz.

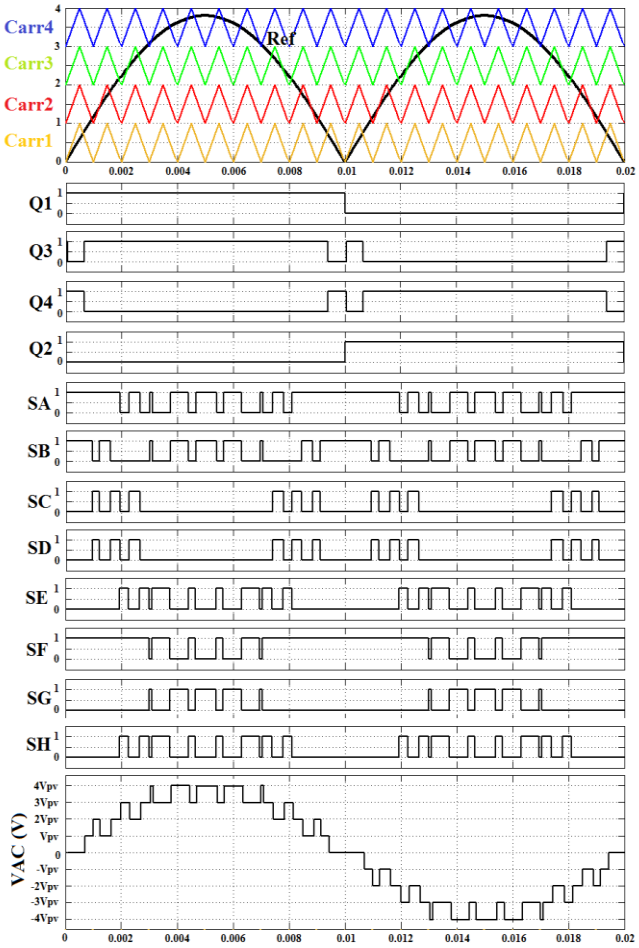

Fig.10. The used PWM structure with the gate pulses

Table 4. The used conditions to activate the power switches with the PWM method

Conditions	ON Switches
(Ref >= Carr4)	SG
NOT SG pulse	SF
(Ref >= Carr3)AND(Ref <= Carr4)	SH and SE
(Ref >= Carr2)AND(Ref <= Carr3)	SD and SC
NOT SE pulse	SA
NOT{(SD pulse) OR (SE pulse)}	SB
{(Ref >= Carr1)AND(Q1 pulse)} OR{(Ref <= Carr1)AND(Q2 pulse)}	Q3
{(Ref >= Carr1)AND(Q2 pulse)} OR{(Ref <= Carr1)AND(Q1 pulse)}	Q4

*In the case of the fundamental switching method, the triangular carrier signals are replaced with constant values with the same amplitude and having an offset equal to their amplitude. As a result the shape of the output AC voltage will be similar to the waveform seen in "Fig.9".

3. Control Method of the Studied PV System for Standalone Applications with MPPT and Voltage Regulation

Maximum power point tracking (MPPT) is a method to extract the maximum power energy available across the solar panels under all climatic condition. In this study, the used MPPT algorithm is Perturb and Observe (P&O). Despite some problems that can be produced by this method, like oscillations across the maximum power point (MPP), it was used for its simplicity and easy implementation. But other more effective methods can be implemented to achieve better performance [20] [21].

The used MPPT method requires just sensing Vpv and Ipv from solar panels and operates by perturbing Vpv to ensure maximum power energy. "Figure 11" shows the flowchart of this method [22] [23] [24].

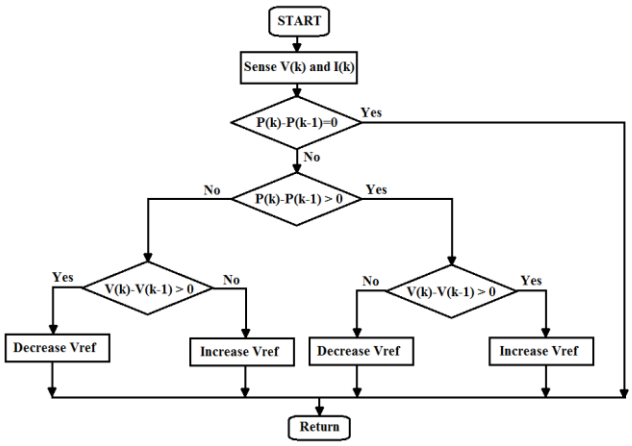

Fig.11. The flowchart of the MPPT algorithm

For standalone applications without storage batteries, the use of the MPPT will help the proposed PV system to deliver maximum power energy to the loads. However, the output AC voltage will not be fixed at a specific voltage, because it will change depending on the value of loads and the delivered power energy from solar panels. In order to fix a nominal voltage that the system never exceeds under any change in climatic conditions and loads, a closed loop voltage control system will be added with the MPPT control method. "Figure 12" shows the flowchart of the proposed control method, and "Fig.13" shows the implementation of the proposed control method with the studied PV system. A low pass filter composed of one inductor (LF) and one capacitor (CF) is added to the PV system to obtain sinusoidal voltage across loads; this will make easier to calculate the RMS values and minimize harmonics.

In order to analyze the operation of the proposed control method, the chosen autonomous load was designed to absorb a specific power energy P-load under an AC voltage with a specific RMS value (VRMS-Ref).

Case1: When the solar panels are under optimal climatic conditions, and the maximum power energy available across solar panels (Pmax-PV) is greater than P-load, in this case, the PV system start to work, and the control system delivers the amplitude AM1 from the MPPT block. When the RMS value of the output AC voltage across the load (VAC-RMS) will be greater than or equal to the specified RMS value (VRMS-Ref) the control system switch from MPPT block to voltage regulation block, as described in "Fig.12", in this case, the control system delivers the amplitude AM2 from the voltage regulation block. AM2 is generated from a classical PI regulator that minimizes the error between the RMS reference and the sensed RMS as shown in "Fig.13".

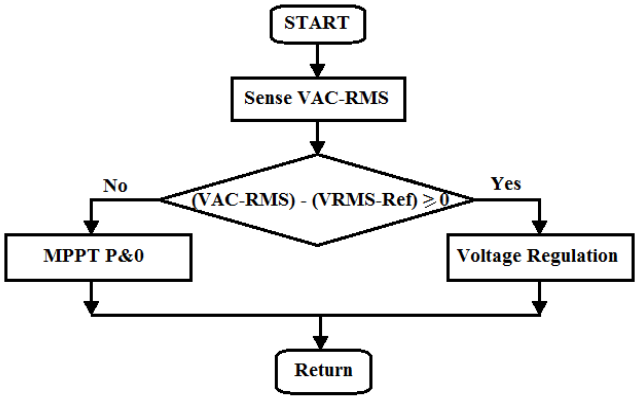

Fig.12. The flowchart of the MPPT with voltage regulation

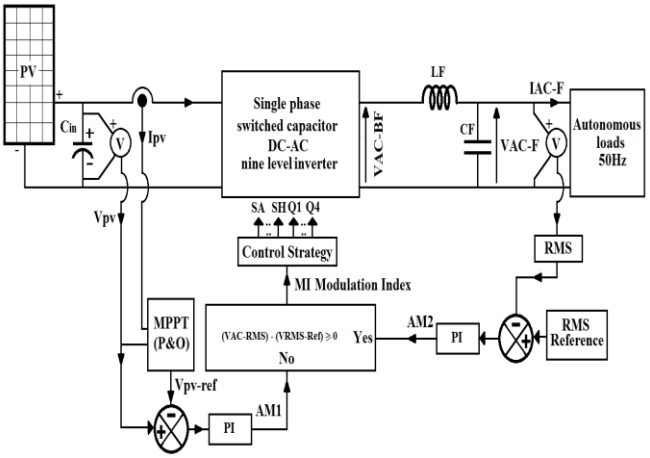

Fig.13. The studied PV system with the proposed control method

Case2: When the maximum power energy available across solar panels is less than P-load, the RMS value of the output AC voltage will never exceed VRMS-Ref. In this case, the PV system will deliver the maximum power energy to the load and the control system delivers the amplitude AM1 from the MPPT block. AM1 is generated from a classical PI regulator that minimizes the error between (Vpv-ref) from the MPPT block and Vpv across solar panels, as shown in "Fig.13". In addition, This PI controller improves the speed of the MPPT method; for that, the response of the studied PV system will be quicker to any change in climatic conditions.

From the two cases, discussed, the proposed control method delivers the appropriate modulation index according to the chosen load and the power energy available across solar panels. For that, the chosen value between the control signals AM1 or AM2 will be multiplied with the unitary

rectified sinusoidal signal and the resulting signal will be compared to four triangular carrier signals in order to generate the corresponding pulses of the inverter based on "Table 3." as shown in "Fig.14".

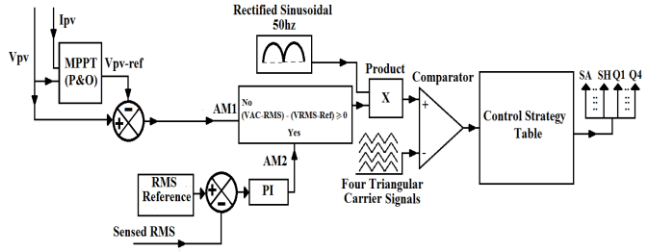

Fig.14. The proposed control method with PWM

The proposed control method combines the advantages of the MPPT and the voltage regulation because:

*If the control system is composed just of voltage regulation block, the PV system will deliver a regulated output AC voltage to the load if Pmax-PV is greater than P-load, but when Pmax-PV is less than P-load, the system try to regulate the output AC voltage by demanding more current from solar panels; as a result, the current Ipv will go to short-circuit current (Isc), and the Vpv will go to zero; this case is to avoid because it can destroy the solar panels.

*if the control system is composed just by MPPT, the PV system will deliver maximum power energy with an output AC voltage less than the optimal voltage for the load as long as Pmax-PV is less than P-load, but when Pmax-PV is greater than P-load, the system will deliver also maximum power energy to the load, however the output AC voltage will exceed the optimal voltage for load, this case is to avoid because loads cannot support a big variation in high voltage.

4. Control Method of the Studied PV System Tied to the Grid with MPPT and Unity Power Factor Correction

In order to inject power energy from the studied PV system into the grid, it's necessary to respect some standard limits dealing with interconnections of PV systems to the electrical network [25] [26] [27]. "Table 5." resumes the most standard limits which will be considered in this paper.

Table 5. The considered standard limits for the proposed PV system tied to the grid

Element	Standard limits
THD of injected current at the fundamental frequency	$\leq 5\%$
Frequency range	$50 \pm 1\text{Hz}$
Power factor ($\cos\varphi$)	> 0.9
Output Voltage range	$196\text{V} < VRMS < 253V$

"Figure 15" shows the proposed control method used with the PV system tied to the grid. A simple filter L is added to the PV system to minimize harmonics contained in the injected current [28].

The MPPT block will help the studied PV system to inject the maximum power energy available across solar panels into the grid, by fixing Vpv to a value which will be increased to 4Vpv with the dc-dc converter in order that the output AC voltage from the PV system (VAC-sys) will be greater than the grid voltage (VG), in another way to respect the condition described in "Eq. (7)" [28] [29].

$$(\text{VAC. sys RMS}) > \sqrt{2} * (\text{VG. RMS}) \qquad (7)$$

To ensure that the injected current will be sinusoidal and in phase with the grid voltage (VG) and the power factor is near to 1, the difference between (Vpv-ref) from the MPPT block and Vpv across solar panels will be corrected with a classical PI regulator which will deliver the magnitude (m) of the reference injected current. This magnitude (m) will be multiplied with the image of the grid voltage to form the reference injected AC current (IAC-ref) which will be compared to the injected current into the grid (IAC-sys) and the error signal will be rectified with a PI regulator which will deliver the control signal u for the PV system.

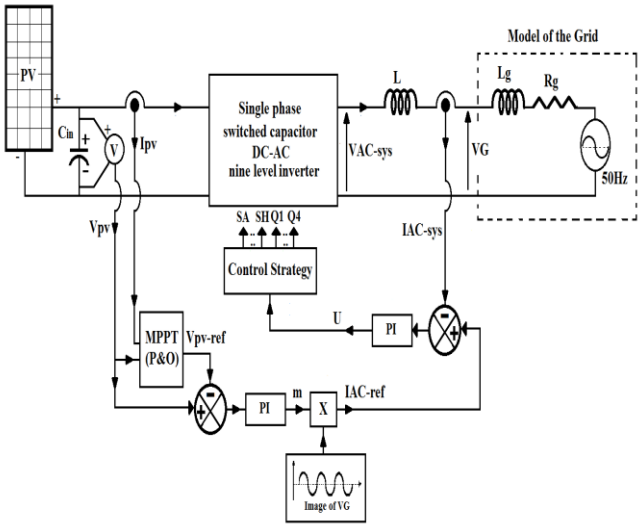

Fig.15. The studied PV system tied to the grid with the proposed control method

The proposed control method ensures that the PV system delivers maximum power energy available and the injected current is sinusoidal in form and in phase with the grid voltage, by delivering the control signal U. This signal will be rectified and compared to four triangular carrier signals in order to generate the corresponding pulses of the inverter based on "Table 3." as shown in "Fig.16".

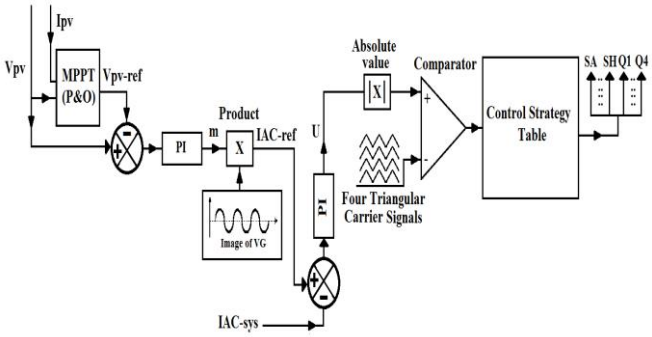

Fig.16. The proposed control method with PWM

5. Simulation Results

5.1. MPPT with voltage regulation control method: Simulation results with inductive load and different irradiation levels and temperatures levels

The MPPT with the voltage regulation method for stand-alone applications applied on the studied PV system as shown previously in "Fig.13" is tested on MATLAB / SIMULINK. "Table 6." shows the values of the main elements used in this test.

Five solar panels coupled in series are used as a DC source, which their electrical characteristics are already indicated in "Table 1.". The values of the capacitors C1, C2 and C3 are based on the study presented in [13] [14] and also from the experimental tests with a fabricated laboratory prototype.

Table 6. The values of the main elements of the PV system in this test

Elements	Values
N° of Solar panels in series	5
Cin	300µF
C1=C2=C3	750µF
FCarr signals	15Khz
FAC voltage	50hz
Low pass filter	LF=70mH ; CF=10µF
RMS reference	220V

"Figure 17" shows the chosen climatic conditions for this test with the maximum power energy available across the five solar panels. When the irradiation level is 1000W/m^2 and the temperature is 25°C the maximum power energy available is 303W, and when the irradiation level change to 800W/m^2 and temperature change to 20°C the maximum power energy available is 246W.

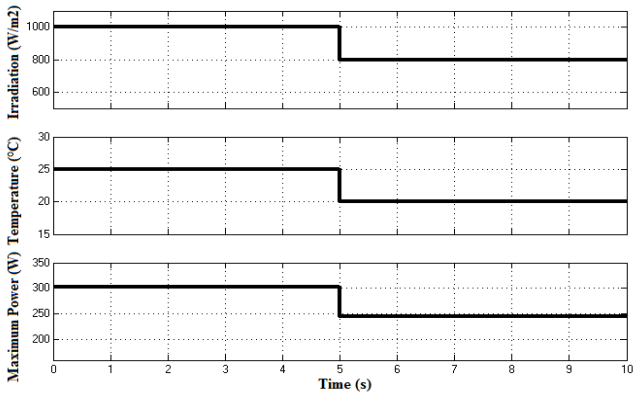

Fig.17. The chosen climatic conditions with maximum power energy across the solar panels

The chosen inductive load is designed to absorb power energy between 303W and 246W under 220V RMS; for this, the parameters of this load are RL= 125Ω; L= 0.24H; Cos φ= 0.85. This load will absorb 280W under 220V RMS/ 50Hz.

"Figure 18" shows the simulation results of the maximum power energy available across solar panels (Pmax-PV) and the power energy delivered to the PV system (P-sys). From 0 to 5s when the irradiation is 1000W/m^2, the five solar panels deliver 290W to the PV system. At 5s when the irradiation changes to 800W/m^2, the five solar panels deliver 246W which is the maximum power energy available.

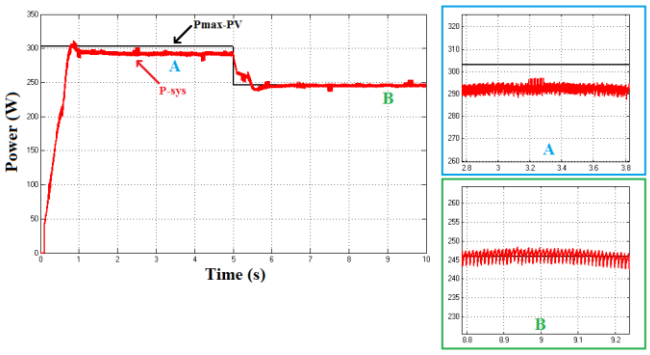

Fig.18. Pmax-PV with P-sys in Watt

"Figure 19" shows the output voltage (Vpv) and output current (Ipv) from solar panels under this test. From 0 to 5s, the average value of voltage from solar panels is about 89.5V, this value is due to the working of the voltage regulation control block, and the average value of current is 3.25A; for that (P-sys = 290W). At 5s when irradiation changes to 800W/m2, the average value of voltage decrease to 84V, this value is fixed from the MPPT block, and the average value of current decrease to 2.94A; for that (P-sys = 246W).

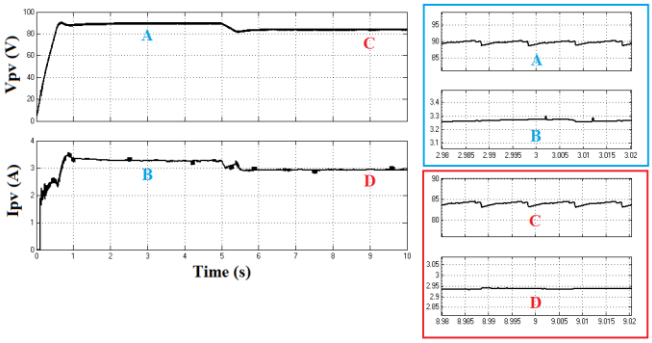

Fig.19. Voltage and current from solar panels

"Figure 20" shows the output AC voltage across the load before the filter (VAC-BF). The PV system delivers nine levels output voltage with a frequency of 50 Hz to the inductive load.

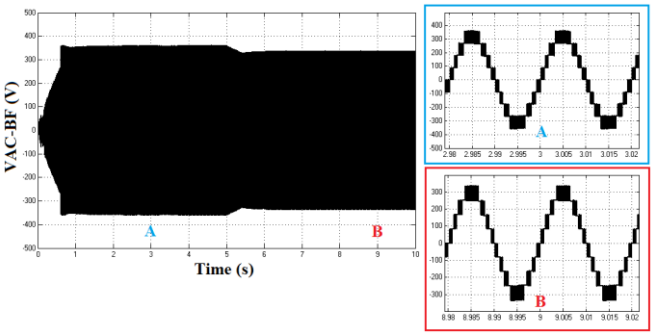

Fig.20. The output AC voltage from PV system before the filter

"Figure 21" shows the output AC voltage (VAC-F) and the output AC current (IAC-F) across the load after the filter. By using the low pass filter, the voltage and current supplied to the inductive load are sinusoidal with low ripples.

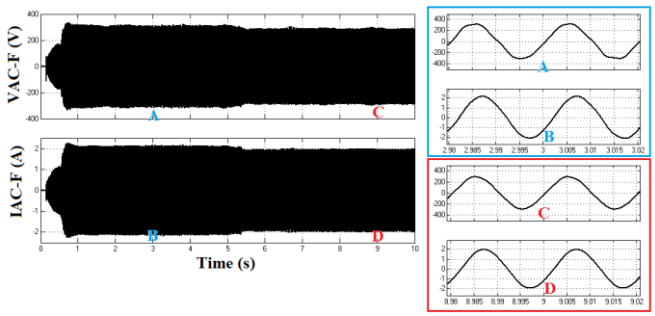

Fig.21. The output AC voltage and the output AC current from PV system after filter

"Figure 22" shows the RMS value of the output AC voltage (VAC-RMS) across the load with the RMS reference (VRMS-Ref) and the RMS value of the output AC current (IAC-RMS). From 0 to 5s the maximum power energy available across solar panels Pmax-PV is greater than P-load; for that the control system work in voltage regulation mode and the load is working under 220V RMS and 1.5A RMS (P-load= 280W). From 5 to 10s, when the irradiation decrease to 800W/m2, Pmax-PV decrease to a value less than P-load; for that the control system work in MPPT mode and the load is working just under 203V RMS and 1.38A RMS (P-load= 238W) because the maximum power energy available across panels is 246W.

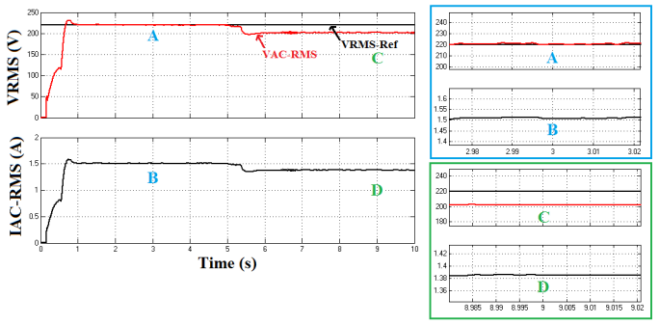

Fig.22. The RMS values of the output AC voltage and the output AC current from PV system

"Figure 23" shows the control signals obtained from the MPPT block (AM1) and from the voltage regulation block (AM2). From 0 to 5s, Pmax-PV is greater than P-load, the PV system starts to work and try to deliver the maximum power energy for the load, and the control signal that will be used with PWM algorithm is AM1 from MPPT block. The voltage regulation block will not be used and work in saturation mode (AM2 in the limit). At 0.84s, VAC-RMS will be greater than VRMS-Ref, at this time the control system switch from MPPT block to voltage regulation block, and the control signal that will be used with PWM algorithm is AM2. The MPPT block will not be used and work in saturation mode (AM1 in the limit). At 5s, Pmax-PV decrease to a value less than P-load, in this case, VAC-RMS will never reach VRMS-Ref, the control system switch from voltage regulation mode to MPPT mode, and the control signal that will be used with PWM algorithm is AM1. The voltage regulation block will not be used and work in saturation mode (AM2 in the limit).

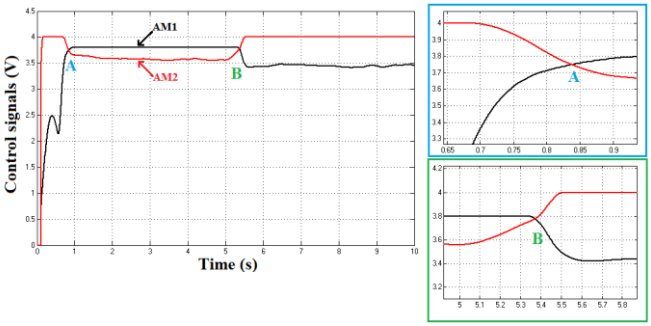

Fig.23. The control signals AM1 and AM2 from the proposed control method

"Figure 24" shows the resulting signal (AM) deduced from (AM1 and AM2) that will be used with PWM algorithm. From 0 to 0.84s, AM will take a value which increases from 0 to 3.7V. From 0.84s to 5s, AM will take a value of 3.55V. And from 5s to 10s, AM will take a value of 3.45V.

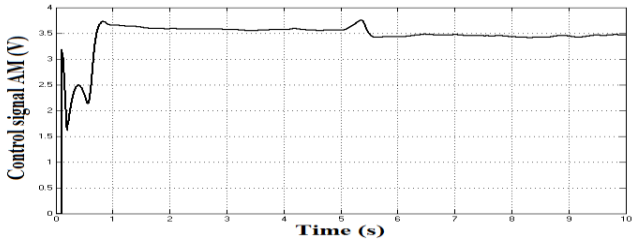

Fig.24. The resulting signal AM used with PWM

From all the presented results, if the power energy available across solar panels is more than the energy required for the load, the control system will regulate the output voltage at a nominal voltage (220V RMS) with the help of voltage regulation block. When the energy across solar panels decreases to a value less than the energy required for the load, the control system tries to give control signals for the PV system in order to deliver the maximum power energy with the help of the MPPT block. As a result, the control system delivers a modulation index to the PV system according to the power energy available across solar panels and the power energy needed for the load. The proposed control method with the studied PV system is a good solution for standalone applications, and especially for PV pumping systems without batteries, where the important thing is to pump water at each time of day.

5.2. MPPT with voltage regulation control method: Simulation results with single phase induction motor and fundamental switching method

In this test, four solar panels coupled in series (4*PV) are used as a DC source, the load will be a single phase induction motor with a rated power of 130W and a power factor of Cos φ=0.4 (the objective of using a motor with a smaller power factor is for testing the proposed PV system in critical conditions) [30]. For the control method, PWM algorithm is replaced by the fundamental switching method. The climatic condition will be fixed at 1000W/m^2 and 25°C; for that the maximum power energy which will be available

across the four solar panels is 242W. The low pass filter will not be used. “Table 7.” resumes the values of the main elements of the PV system used in this test.

Table 7. The values of the main elements of the PV system in this test

Elements	Values
N° of Solar panels in serie	4
Cin	300µF
C1=C2=C3	750µF
FAC voltage	50hz
RMS reference	220V
Motor	P=130W ; Cosφ=0.4

“Figure 25” shows the simulation results of the maximum power energy available across solar panels (Pmax-PV) and the power energy delivered to the PV system (P-sys). From 0 to 0.5s, the four solar panels deliver 206W to the PV system to let the motor to start. And from 0.5s to 10s, when the motor is already starting, the four solar panels deliver 136W to the PV system.

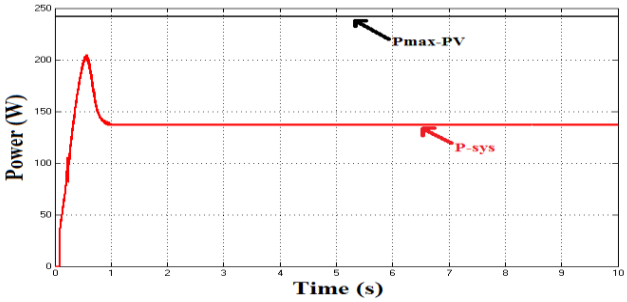

Fig.25. Pmax-PV with P-sys in Watt

“Figure 26” shows the output voltage (Vpv) and output current (Ipv) from solar panels under this test. From 0 to 0.5s, when the motor is starting, the average value of voltage is 78V and the average value of current is about 2.65A (P-sys=206W); theses two values are due to the working of MPPT block. From 0.5s to 10s, the average value of voltage from solar panels is about 81V and the average value of current is about 1.69A (P-sys=136W), theses two values are due to the working of the voltage regulation control block. The shape of the voltage is due to the charging and discharging of capacitors.

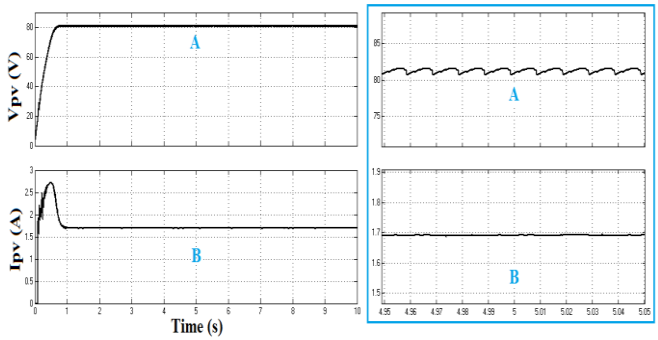

Fig.26. Voltage and current from solar panels

“Figure 27” shows the output AC voltage (VAC-M) and the output AC current (IAC-M) across the single phase induction motor. The PV system delivers an AC voltage with nine levels to the single phase induction motor, and the output AC current is sinusoidal just by using fundamental switching method.

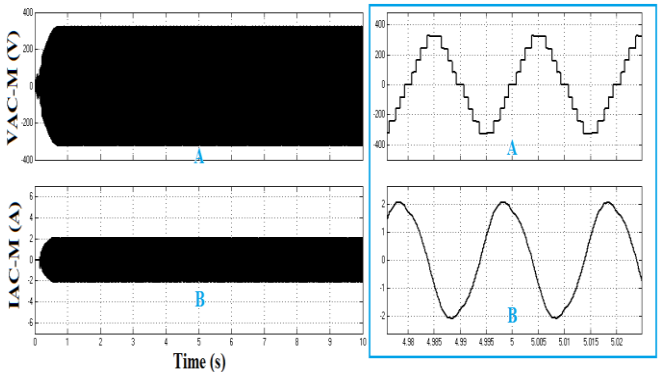

Fig.27. Voltage and current across the motor

“Figure 28” shows the THD of the output AC voltage (VAC-M) and the THD of the output AC current (IAC-M) across the single phase induction motor. The output AC voltage is near to a sinusoidal in shape and its quarter wave is symmetrical across the time's axis, as a result, the even harmonics are absent. The important odd harmonics (3rd, 5th, 7th, 9th and 11th) are less than 8%, and the THD of the output voltage is 12.86%. For the output AC current, the even harmonics are absent, the important odd harmonics are less than 5.5%, and the THD is 5.32%. At the fundamental frequency (50Hz) the induction motor work under 220.05V RMS and 1.48A RMS; for that the consumed power energy is 130.26W.

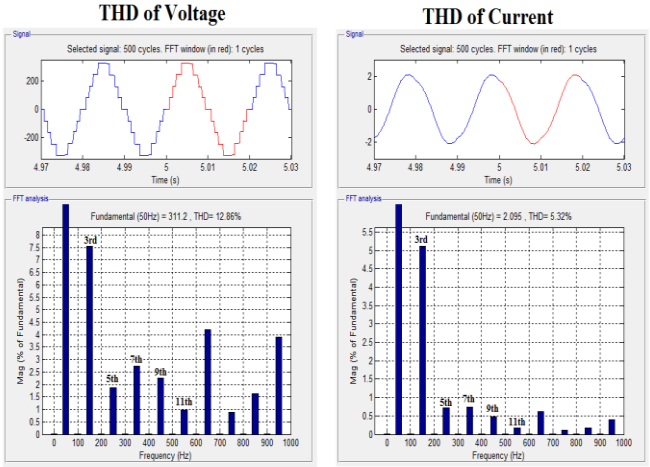

Fig.28. THD of voltage and current across the motor

“Figure 29” shows the control signals obtained from the MPPT block (AM1) and from the voltage regulation block (AM2). From 0 to 10s, Pmax-PV is greater than P-load; the PV system starts to work and try to deliver the maximum power energy to the load, and the control signal that will be used with PWM algorithm is AM1 from MPPT block. At 0.5s, VAC-RMS will be greater than VRMS-Ref, at this time the control system will switch from MPPT block to voltage regulation block and the control signal that will be used with PWM algorithm is AM2.

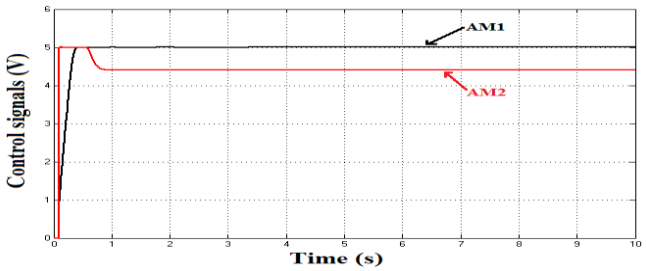

Fig.29. The control signals AM1 and AM2 from the proposed control method

"Figure 30" shows the resulting signal (AM) deduced from (AM1 and AM2) that will be used with PWM algorithm. From 0 to 0.5s, AM will take a value which increases from 2.8 to 5V. From 0.5s to 10s, AM will take a value of 4.4V.

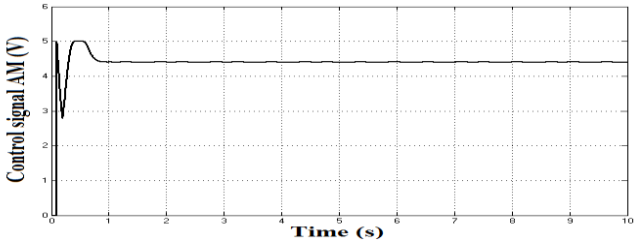

Fig.30. The resulting signal AM used with fundamental switching method

In this test, the MPPT with voltage regulation method was applied to the proposed PV system supplying power energy to a single phase induction motor. The simulations results prove the performance of the proposed control method. In the case of PV pumping system applications with induction motor, it's not longer necessary to use low pass filter with the studied inverter because the output AC current will be sinusoidal in shape and the system deliver fewer harmonics with good results just by using fundamental switching method.

5.3. Simulation results of the studied PV system tied to the grid with MPPT and unity power factor correction

The MPPT with unity power factor correction method applied on the studied PV system tied to the grid as shown previously in "Fig.15" is tested on MATLAB / Simulink. "Table 8." shows the values of the main elements used in this test.

Table 8. The values of the main elements of the PV system

Elements	Values
N° of Solar panels in serie	5
Cin	300µF
C1=C2=C3	750µF
FCarr signals	15Khz
Filter	L=20mH
Model of the Grid	VG-rms= 220V RMS; Lg=50e-6H; Rg=1Ω; F= 50Hz

"Figure 31" shows the chosen climatic conditions for this test with the maximum power energy available across the five solar panels. When the irradiation level is 1000W/m2 and the temperature is 25°C the maximum power energy available is 303W. When the irradiation level is 800W/m2 and the temperature is 20°C, the maximum power energy available is 246W. And when the irradiation level is 600W/m2 and temperature is 18°C, the maximum power energy available is 184W.

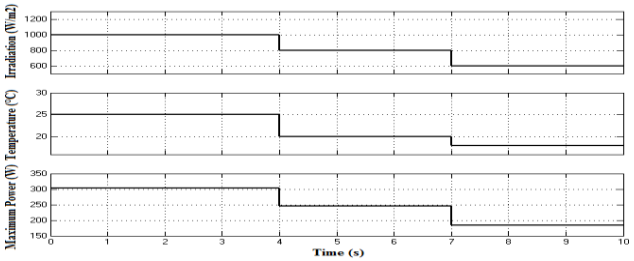

Fig.31. The chosen climatic conditions with maximum power energy across the solar panels

"Figure 32" shows the simulation results of the maximum power energy available across solar panels (Pmax-PV) and the power energy delivered to the PV system (P-sys) under this test. From 0 to 10s although the irradiation levels change with temperature, the five solar panels supply the maximum power energy available to the grid through the PV system.

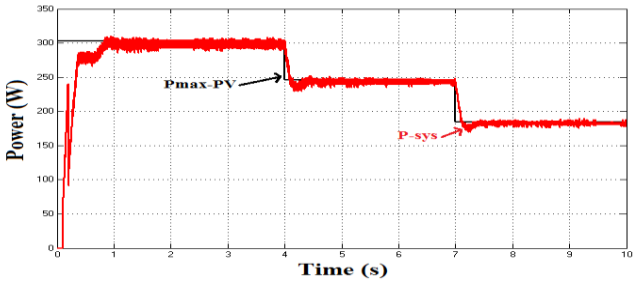

Fig.32. Pmax-PV with P-sys in Watt

"Figure 33" shows the output voltage (Vpv) and output current (Ipv) from solar panels under this test. From 0 to 4s, the average value of voltage from solar panels is about 82.5V and the average value of current is 3.6A. At 4s when irradiation changes to 800W/m2, the average value of voltage remains equal to 82.5V and the average value of current decrease to 2.9A. At 7s when irradiation changes to 600W/m2, the average value of voltage still equal to 82.5V and the average value of current decrease to 2.2A.

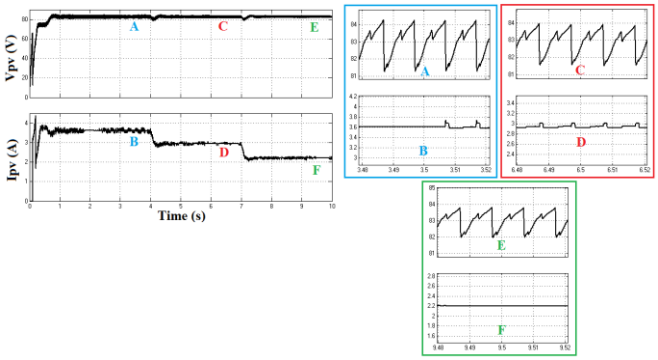

Fig.33. Voltage and current from solar panels

"Figure 34" and "Fig.35" show respectively the form and the RMS value of the output voltage (VAC-sys) at the AC terminal of the PV system. From 0 to 10s the PV system delivers nine levels output voltage with a frequency of 50 Hz and an RMS value of 225V. Despite the irradiation changes between 0s to 10s, the output AC voltage from the PV system remains constant to a value greater than the AC voltage of the grid; this is very important for injecting current from the PV system to the grid.

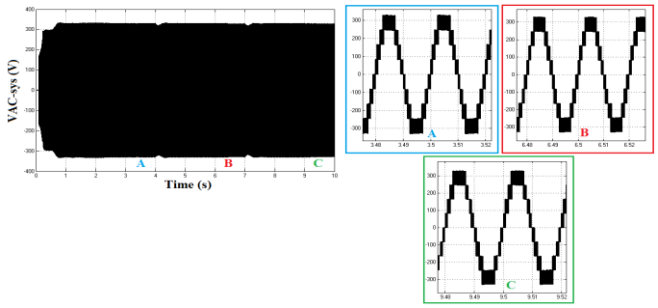

Fig.34. The output AC voltage from the PV system

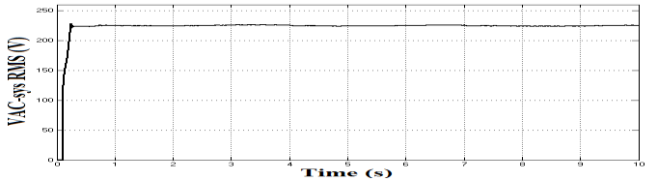

Fig.35. The RMS value of the output AC voltage from the PV system

"Figure 36" shows the output AC voltage (VAC-sys) with the grid voltage (VG). It's clear that the output AC voltage from the PV system is in phase with the grid voltage; this will ensure that the injected current from the PV system will be in phase with the grid voltage.

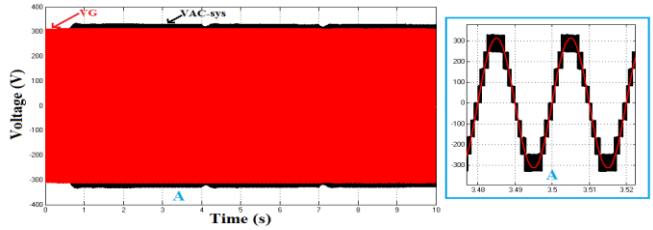

Fig.36. The output AC voltage from the PV system with the grid voltage

"Figure 37" shows the injected output AC current (IAC-sys) into the grid with the grid voltage (VG). The injected current from the PV system into the grid is in phase with grid voltage and the value of the power factor is near to 1.

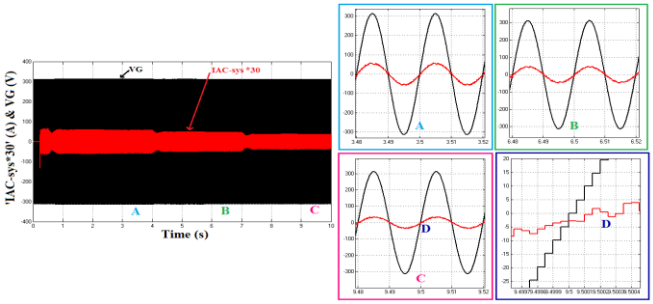

Fig.37. The output AC current from the PV system with the grid voltage

"Figure 38" shows the RMS value of the injected current (IAC-sys) into the grid. From 1 to 4s, the RMS value of the injected current is 1.32A. From 4s to 7s, the RMS value of the injected current decreases to 1.075A. And from 7s to 10s the RMS value of this current another time decrease to 0.8A.

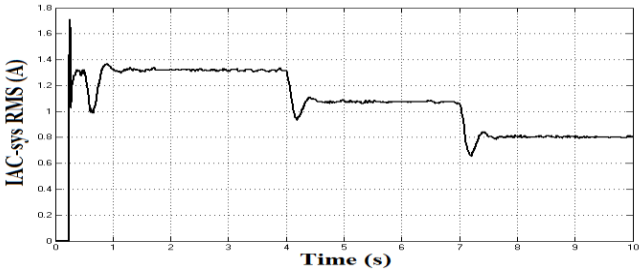

Fig.38. The RMS value of the injected current into the grid

"Figure 39" shows the active power (P-inj) and reactive power (Q-inj) provided from the PV system. From 1 to 4s, P-inj= 291W and Q-inj=30 VAR for that $\cos\varphi = 0.9947$. From 4s to 7s, P-inj=236W and Q-inj=23VAR for that $\cos\varphi = 0.9952$. From 7s to 10s, P-inj=176W and Q-inj=18VAR for that $\cos\varphi = 0.9948$. It's clear that the value power factor is near to 1.

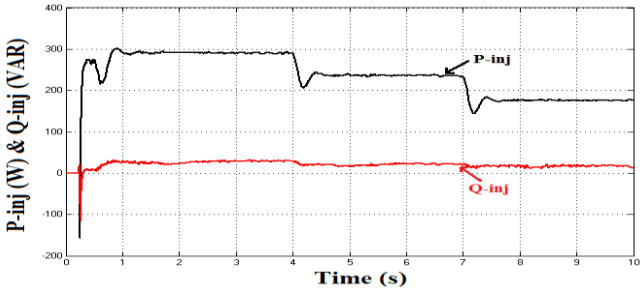

Fig.39. The active power and reactive power provided from the PV system

"Figure 40" shows the THD of the injected current (IAC-sys) into the grid. The important odd harmonics (3rd, 5th, 7th, 9th and 11th) are less than 1%, and the THD is 4.63%.

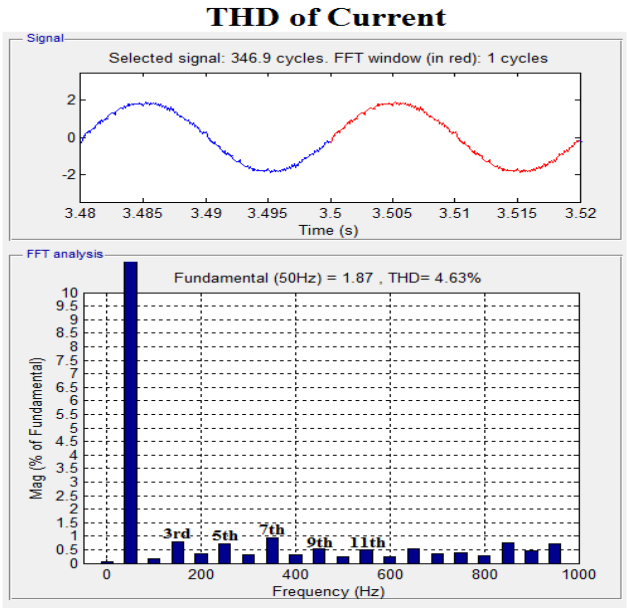

Fig.40. THD of the injected current into the grid

"Figure 41" shows the obtained control signal from the proposed control method. The proposed control method deliver a rectified sinusoidal signal which will be compared to four triangular signals in order to obtain the control pulses of the PV system switches.

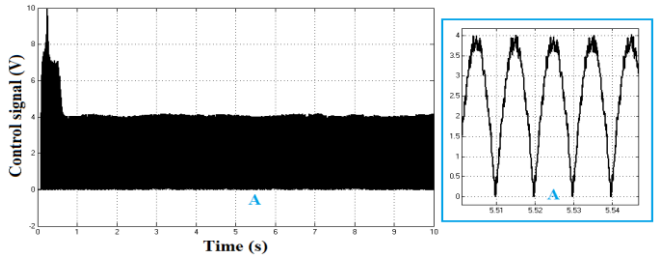

Fig.41. The control signal used with PWM method

In this test, the MPPT with unity power factor correction method was applied to the proposed PV system tied to the grid. The obtained RMS value of the output voltage AC voltage from the proposed PV system is 225V, the THD of the injected current is less than 5%, and the power factor is greater than 0.9. It's clear that the proposed method let the proposed PV system to inject the current into the grid from low power energy by respecting all the standard limits presented in "Table 5."

6. Experimental Results

A laboratory prototype of the used multilevel inverter is fabricated and implemented with a 130W single phase induction motor driving a water pump, and tested in open loop. To generate the switching pulses as described in "Table 3." for the power switches a microcontroller was utilized, and for recording experimental results a digital oscilloscope was used which contains two channels for measuring; channel 1 (ch1) and channel 4 (ch4). "Figure 42" shows the realized laboratory prototype. In this test, stiff DC voltage (Regulated power supply) was used as a DC sources (Vin-DC).

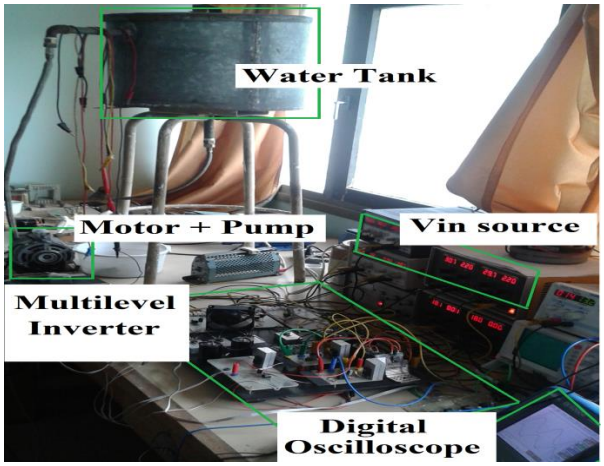

Fig.42. The experimental prototype at the laboratory

"Figure 43" shows the output voltage from DC sources. The DC sources supply voltage with an average value of 79Volt to the experimental setup. The shape and the value of the experimental Vin-DC are close to the simulation result seen in "Fig.26" obtained from solar panels in simulation with closed loop control. The shape of this voltage is due to the charging and discharging of capacitors.

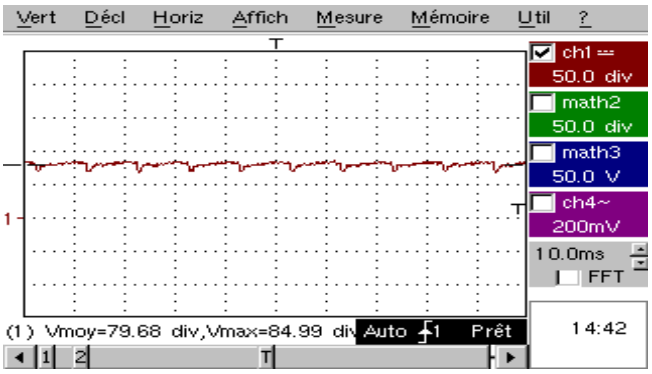

Fig.43. Input voltage (ch1) from Vin source

"Figure 44" and "Fig.45" show the output AC voltage and the output AC current from the fabricated prototype, supplied to the induction motor driving the water pump. The output AC voltage shows 9 levels with an RMS value of 220V (ch1) and a frequency of 50Hz. The RMS value of the AC current is about 1.43A, this value corresponds to 143mV (ch4) because we use a current sensor that gives 100mv for each RMS value of 1A. The shape and the value of the experimental AC voltage and current are also close to the simulation results seen in "Fig.27" and "Fig.28".

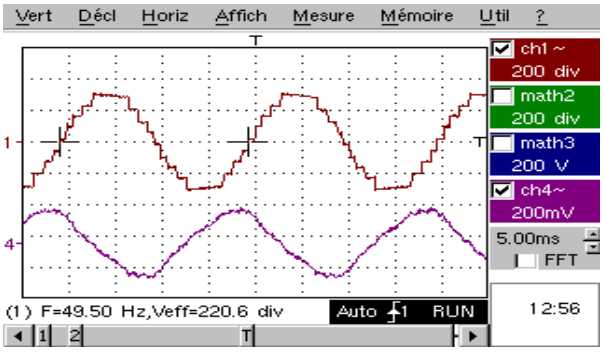

Fig.44. Experimental AC voltage (ch1) and current (ch4), supplied to the induction Motor

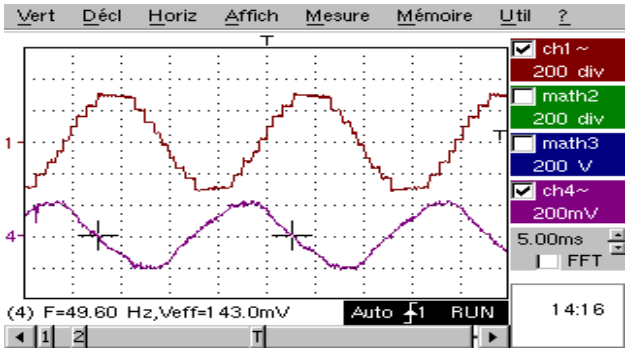

Fig.45. Experimental AC voltage (ch1) and current (ch4), supplied to the induction Motor

"Figure 46" shows the spectral analysis of the output AC voltage and output AC current. The experimental spectrum of the output voltage and current prove that the implemented system delivers fewer harmonics. Also, the experimental spectrum results are close to the simulation results presented in "Fig.28".

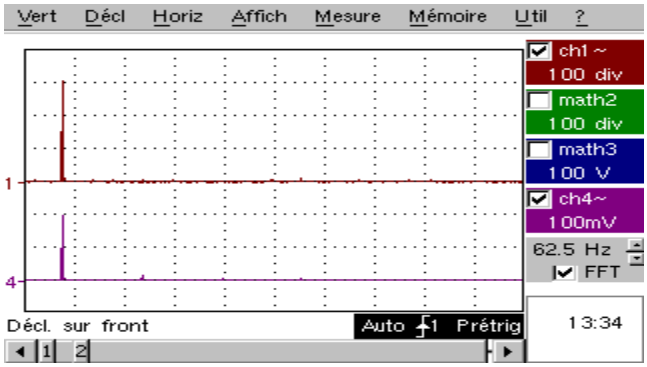

Fig.46. Spectrum of the AC output voltage (ch1) and current (ch4).

These experimental results present the test of the topology of the used multilevel inverter in this paper under industrial value of voltage and frequency (220V RMS. 50Hz). In a future work, all the proposed control methods will be implemented on a DSP card and tested experimentally.

7. Conclusion

In this paper, a detailed study of a single phase switched capacitors nine level inverter for PV system applications was presented. Two control methods were applied to this photovoltaic inverter and tested in the simulation with different cases of PV system application by using a real model of solar panels. Experimental results of a fabricated laboratory prototype for validation of the topology of this multilevel inverter were also presented.

The two main applications of the studied multilevel inverter with the proposed control methods were: PV pumping system and injecting energy from PV sources into the grid by considering the standard limits of interconnections between these two power energy sources.

This multilevel inverter presents many advantages such as; the use of single input dc voltage source from solar panels compared to conventional multilevel inverters, the use of a DC-DC converter without inductors, a THD spectrum with fewer harmonics, high efficiency, good output AC waveforms, and the capability to inject current from PV into the grid from low power energy.

References

[1] U. M. Choi, K. B. Lee, and F. Blaabjerg, "Power electronics for renewable energy systems: Wind turbine and photovoltaic systems," in 2012 International Conference on Renewable Energy Research and Applications (ICRERA), 2012, pp. 1–8

[2] M. Saghaleini, A. K. Kaviani, B. Hadley, and B. Mirafzal, "New trends in photovoltaic energy systems," in 2011 10th International Conference on Environment and Electrical Engineering, 2011, pp. 1–4.

[3] E. Kabalci, Y. Kabalci, R. Canbaz, and G. Gokkus, "Single phase multilevel string inverter for solar applications," in 2015 International Conference on Renewable Energy Research and Applications (ICRERA), 2015, pp. 109–114.

[4] K. K. Gupta, A. Ranjan, P. Bhatnagar, L. K. Sahu, and S. Jain, "Multilevel Inverter Topologies With Reduced Device Count: A Review," IEEE Transactions on Power Electronics, vol. 31, no. 1, pp. 135–151, Jan. 2016.

[5] J. Rodriguez, S. Bernet, B. Wu, J. O. Pontt, and S. Kouro, "Multilevel Voltage-Source-Converter Topologies for Industrial Medium-Voltage Drives," IEEE Transactions on Industrial Electronics, vol. 54, no. 6, pp. 2930–2945, Dec. 2007.

[6] R. A. Krishna and L. P. Suresh, "A brief review on multi level inverter topologies," in 2016 International Conference on Circuit, Power and Computing Technologies (ICCPCT), 2016, pp. 1–6.

[7] S. H. Shehadeh, H. H. Aly, and M. E. El-Hawary, "Photovoltaic multi-level inverters technology," in 2015 IEEE 28th Canadian Conference on Electrical and Computer Engineering (CCECE), 2015, pp. 648–655.

[8] J. Rodriguez, J.-S. Lai, and F. Z. Peng, "Multilevel inverters: a survey of topologies, controls, and applications," IEEE Transactions on Industrial Electronics, vol. 49, no. 4, pp. 724–738, Aug. 2002.

[9] N. Prabaharan and K. Palanisamy, "A comprehensive review on reduced switch multilevel inverter topologies, modulation techniques and applications," Renewable and Sustainable Energy Reviews, vol. 76, pp. 1248–1282, Sep. 2017.

[10] E. Babaei and S. S. Gowgani, "Hybrid Multilevel Inverter Using Switched Capacitor Units," IEEE Transactions on Industrial Electronics, vol. 61, no. 9, pp. 4614–4621, Sep. 2014.

[11] T. Salmi, M. Bouzguenda, A. Gastli, and A. Masmoudi, "MATLAB/Simulink Based Modeling of Photovoltaic Cell," International Journal of Renewable Energy Research (IJRER), vol. 2, no. 2, pp. 213–218, May 2012.

[12] V. V. Ramana, D. Jena, and D. N. Gaonkar, "An Accurate Modeling of Different Types of Photovoltaic Modules Using Experimental Data," International Journal of Renewable Energy Research (IJRER), vol. 6, no. 3, pp. 970–974, Sep. 2016.

[13] M. K. Dave, "Modeling of PV arrays based on datasheet," in 2016 IEEE 1st International Conference on Power Electronics, Intelligent Control and Energy Systems (ICPEICES), 2016, pp. 1–4.

[14] E. Zamiri, N. Vosoughi, S. H. Hosseini, R. Barzegarkhoo, and M. Sabahi, "A New Cascaded Switched-Capacitor Multilevel Inverter Based on Improved Series–Parallel Conversion With Less Number of Components" IEEE Transactions on Industrial Electronics, vol. 63, no. 6, pp. 3582–3594, Jun. 2016.

[15] R. Barzegarkhoo, H. M. Kojabadi, E. Zamiry, N. Vosoughi, and L. Chang, “Generalized Structure for a Single Phase Switched-Capacitor Multilevel Inverter Using a New Multiple DC Link Producer With Reduced Number of Switches,” IEEE Transactions on Power Electronics, vol. 31, no. 8, pp. 5604–5617, Aug. 2016.

[16] P. Natarajan and P. K, “Investigation of single phase reduced switch count asymmetric multilevel inverter using advanced pulse width modulation technique,” International Journal of Renewable Energy Research (IJRER), vol. 5, no. 3, pp. 879–890, Sep. 2015.

[17] A. Edpuganti and A. K. Rathore, “A Survey of Low Switching Frequency Modulation Techniques for Medium-Voltage Multilevel Converters,” IEEE Transactions on Industry Applications, vol. 51, no. 5, pp. 4212–4228, Sep. 2015.

[18] Y. Sinha and A. Nampally, “Modular multilevel converter modulation using fundamental switching selective harmonic elimination method,” in 2016 IEEE International Conference on Renewable Energy Research and Applications (ICRERA), 2016, pp. 736–741.

[19] M. A. Sayed, M. Ahmed, M. G. Elsheikh, and M. Orabi, “PWM Control Techniques for Single-Phase Multilevel Inverter Based Controlled DC Cells,” Journal of Power Electronics, Vol. 16, No. 2, pp. 498-511, March 2016.

[20] M. B. Smida and A. Sakly, “A comparative study of different MPPT methods for grid-connected partially shaded photovoltaic systems,” International Journal of Renewable Energy Research (IJRER), vol. 6, no. 3, pp. 1082–1090, Sep. 2016.

[21] M. Heidari, “Improving Efficiency of Photovoltaic System by Using Neural Network MPPT and Predictive Control of Converter,” International Journal of Renewable Energy Research (IJRER), vol. 6, no. 4, pp. 1524–1529, Dec. 2016.

[22] P. Kinjal, K. B. Shah, and G. R. Patel, “Comparative analysis of P O and INC MPPT algorithm for PV system,” in 2015 International Conference on Electrical, Electronics, Signals, Communication and Optimization (EESCO), 2015, pp. 1–6.

[23] S. Ganesan, R. V, and U. S, “Performance Improvement of Micro Grid Energy Management System using Interleaved Boost Converter and P&O MPPT Technique,” International Journal of Renewable Energy Research (IJRER), vol. 6, no. 2, pp. 663–671, Jun. 2016.

[24] R. Raedani and M. Hanif, “Design, testing and comparison of P amp;O, IC and VSSIR MPPT techniques,” in 2014 International Conference on Renewable Energy Research and Application (ICRERA), 2014, pp. 322–330.

[25] S. B. Kjaer, J. K. Pedersen, and F. Blaabjerg, “A review of single-phase grid-connected inverters for photovoltaic modules,” IEEE Transactions on Industry Applications, vol. 41, no. 5, pp. 1292–1306, Sep. 2005.

[26] A. K, V. D, and P. K, “Recent advances and control techniques in grid connected PV system – A review,” International Journal of Renewable Energy Research (IJRER), vol. 6, no. 3, pp. 1037–1049, Sep. 2016.

[27] M. H. Abbasi, A. Al-Ohaly, Y. Khan, and H. M. Hasainen, “Design phases for grid connected PV system,” in 2014 International Conference on Renewable Energy Research and Application (ICRERA), 2014, pp. 684–688.

[28] M. A. Sayed, M. G. Elsheikh, M. Orabi, E. M. Ahmed, and T. Takeshita, “Grid-connected single-phase multi-level inverter,” in 2014 IEEE Applied Power Electronics Conference and Exposition - APEC 2014, 2014, pp. 2312–2317.

[29] N. A. Rahim, K. Chaniago, and J. Selvaraj, “Single-Phase Seven-Level Grid-Connected Inverter for Photovoltaic System,” IEEE Transactions on Industrial Electronics, vol. 58, no. 6, pp. 2435–2443, Jun. 2011.

[30] R. Darbali-Zamora, D. A. Merced-Cirino, A. J. Díaz-Castillo, and E. I. Ortiz-Rivera, “Single phase induction motor alternate start-up and speed control method for renewable energy applications,” in 2014 International Conference on Renewable Energy Research and Application (ICRERA), 2014, pp. 743–748.